

PAPER • OPEN ACCESS

Analysis of the Francis turbine upper-part-load pulsation Part I – Experimental results vs. hydro-acoustic model

To cite this article: P K Dörfler 2019 *IOP Conf. Ser.: Earth Environ. Sci.* **240** 052022

View the [article online](#) for updates and enhancements.



IOP | ebooks™

Bringing you innovative digital publishing with leading voices to create your essential collection of books in STEM research.

Start exploring the **collection** - download the first chapter of every title for free.

Analysis of the Francis turbine upper-part-load pulsation

Part I – Experimental results vs. hydro-acoustic model

P K Dörfler

Consulting engineer, Hydro adviser LLC, Zurich (Switzerland)

E-mail: contact@hydroadviser.ch

Abstract. An acoustical model for wave propagation on a cavitating vortex flow bounded by a cylindrical wall is applied to the upper-part-load pressure pulsation of some Francis turbines with high specific speed. Due to the high frequency, the pressure amplitude has an important radial gradient. Together with the precession of the eccentric vortex axis, this gradient entails a modulation of pressure amplitude at each point of the draft tube wall; this causes the asynchronous side bands in the pressure spectra. Experiments confirm that the oscillation is synchronous within one cross section. Oval deformation of the cavity, occasionally observed, does not show in the phase of wall pressure; it is not relevant for the oscillation mechanism. The typical amplitude and phase relationships upstream and downstream of the turbine are also properly described by the simplified model. The upper-part-load pulsation occurs only in presence of a cavitating part-load vortex to which it is superimposed. Like the full-load surge, it occurs in a load range with relatively high absolute mass-flow gain. The frequency is always much higher than the precession and lowest natural frequency. Model tests reproduced the pulsation and its relative frequency in a wide range of the test head, which means it does not depend very much on the response of the test installation. The pressure at the upper and lower end of the vortex has roughly opposite phase. In some tests the pressure amplitude in the draft tube cone was smaller than upstream and downstream. Like the reversal of phase, this is a consequence of the mode shape. All these facts suggest this pulsation is self-excited and based on a half-wavelength standing wave on the cavitating flow region. The mechanism of self-excitation is analyzed in Part II of the study.

1. Introduction

The flow downstream of the runner of a Francis turbine has a swirling component if the discharge differs from its design value. Due to this swirl, every Francis turbine has some range of partial load operation where the draft tube flow develops into a corkscrew-shaped vortex, the ‘draft-tube rope’; typically this is the case between 50 and 85% of best-efficiency discharge. The helical rope structure performs a slow rotation about the draft tube axis at a frequency of 0.2 to 0.4 times runner rotation, producing variations of pressure and discharge.

Since the early 1990s several researchers [2][3] reported about a different kind of pulsation that occurred additionally, most frequently between 70 and 85% of best-efficiency discharge. This phenomenon, called high-partial-load pulsation or 80%-pulsation, has been object of various studies because alarming amplitudes have been observed in some cases. It only occurs if the rope has some amount of cavitation. Depending on the draft tube pressure level, frequencies f_c between 1 and 4 times runner frequency n have been reported (Table 2). Pressure spectra from the draft tube wall are composed of several narrow bands, the frequency bands always differing by integer multiples of the



vortex precession frequency f_v . For example, spectra from 2 opposite locations are shown in Figure 1. In this example [1], the relative frequencies are $f_v/n=0.32$ for vortex precession and $f_c/n=2.63$ for the main band of the 80% pulsation. The corresponding signals in time domain are shown in Figure 4.

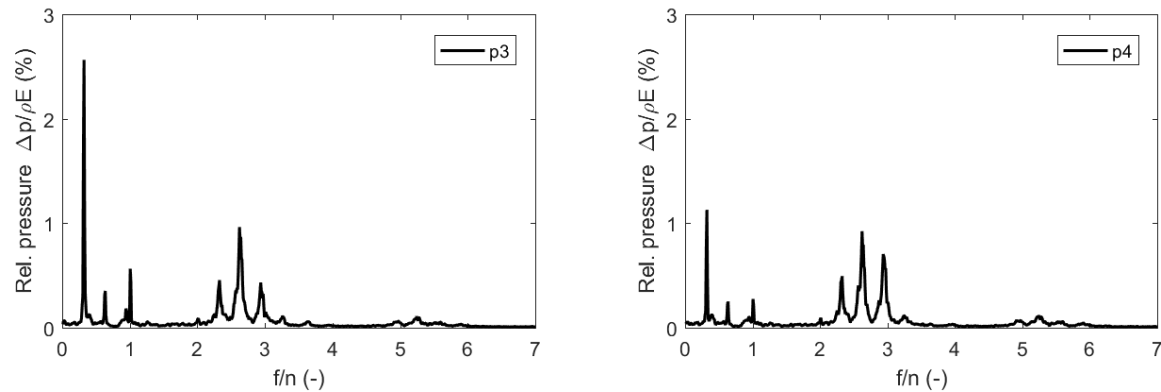


Figure 1. Draft tube pressure spectra [1] p3=cone left and p4=cone right, for conditions see Table 2/ case 6

In a model test with a very distinct pulsation, Arpe [4] measured and analyzed the distribution of amplitude and phase over the entire surface of the draft tube. He and other authors ([2][6]) found that the main frequency band of the pulsation has synchronous character; the pulsations at $f=f_c$ measured at all pressure sensors in a cross section are in phase. He concluded that the banded frequency pattern is due to some process of modulation with the high-partial-load pulsation as a carrier frequency.

Until today there is no satisfactory explanation for the occurrence and particular features of this pulsation phenomenon. The present analysis attempts to give such an explanation using a simplified acoustic model of wave propagation on a cavitating vortex (section 2); the properties of this model are compared to available experimental results (section 3) to check its validity. Part II [13] clarifies the way of oscillation energy supply and the reasons for the particular conditions of occurrence.

2. Simplified theory of interior pressure pulsation

The objective is to study very basic properties of wave propagation on a bounded cylindrical vortex; the helical shape of the draft tube rope is reduced to a straight axial shape, and the axial variation of cross section and mean pressure is not considered. Due to these strong simplifications, an analytical solution can be described in section 2.1. An example using absolute data from a model test is presented in 2.2. The results are used in section 2.3 to explain the origin of the spectral side bands.

2.1. Acoustical model

Wave propagation on a cavitating vortex has been extensively studied by experiments as well as analytically. For the unbounded case, without a rigid wall, solutions are available for a number of more or less realistic vortex models. For the unbounded potential vortex Bosschers [9] published the analytical solution; later the deduction has been extended to certain viscous vortex types and experimentally validated [10]. In the following, the analytical treatment will be adjusted to hold for a potential vortex bounded by a rigid concentric cylindrical wall. Bosschers' deduction need not be repeated here but the main steps are mentioned using his notation. The small-scale velocity fluctuations in time as well as in radial, axial and circumferential direction are represented as perturbations of a velocity potential ϕ . Separation of variables is applied; the influences of time (t) and of the axial and circumferential coordinate (z and θ) are assumed harmonic while due to the cylindrical geometry the radial term $\phi(k,r)$ is a Bessel function. The velocity perturbation potential thus becomes

$$\tilde{\phi} = \phi(k,r)e^{i(k_z z + n\theta - \omega t)} \quad (1)$$

The integer-valued parameter n describes the azimuthal variations of pulsation. In Figure 2 the mode shapes (e.g., displacement of the cavity surface) for the modes $n=0$, 1 and 2 are visualized.

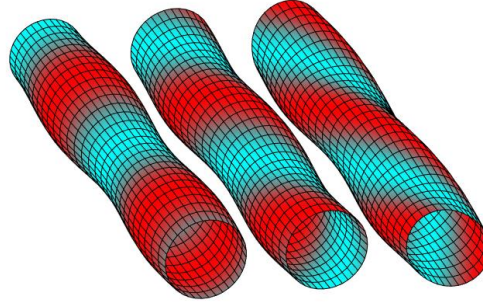


Figure 2. Deformation of cavity by modes $n=0$ (breathing), $n=1$ (helix), and $n=2$ (ovalization)

The acoustic wave number k in the fluid moving with velocity W in direction z is given by

$$k^2 = \frac{1}{c^2}(\omega - Wk_z)^2 = k_r^2 + k_z^2 \quad (2)$$

For the low frequencies ω and velocities W of interest, the acoustic wavenumber k is very small compared to the axial wavenumber k_z ; this will be demonstrated in 2.2. As a consequence the radial wavenumber k_r is always imaginary and therefore $\phi(k_r r)$ has to be composed of modified (non-oscillating) Bessel functions. The solution for the unbounded case [9] is the modified Bessel function of second kind K_n . In case of the draft tube vortex, there is a finite ratio between pipe wall radius r_w and mean cavity radius r_c . In order to fulfil the outer boundary condition $u_r(r_w)=0$, $\phi(k_r r)$ should be a linear combination of the functions $K_n(ik_r r)$ and $I_n(ik_r r)$,

$$\phi(k_r r) = \Phi \cdot (K_n(ik_r r) + \alpha \cdot I_n(ik_r r)), \quad \alpha = -K_n'(ik_r r_w) / I_n'(ik_r r_w) \quad (3)$$

The kinematic boundary condition describing the movement of the cavity surface yields a relationship between the variation of the potential (Φ) and the radial displacement of the surface (R):

$$\Phi k_r \phi'(k_r r_c) + iR(\omega - Wk_z - n\Omega) = 0 \quad (4)$$

In equation (3), Ω indicates the angular frequency of flow rotation at the cavity surface, $\Omega = V_c / r_c$ for the assumed potential vortex. Using the Bernoulli equation, the condition of constant pressure at the cavity surface provides an additional relationship

$$(Wk_z - \omega + n\Omega)\Phi \phi(k_r r_c) + iR\Omega^2 r_c = 0 \quad (5)$$

The dispersion relation, defining the relationship between frequency and wave number, is obtained from equations (3) and (4) after some rearranging, and introducing the parameter $\kappa = k_r r_c$

$$\omega = Wk_z + \Omega \cdot \left(n \pm \sqrt{\frac{-\kappa \phi'(\kappa)}{\phi(\kappa)}} \right) \quad (6)$$

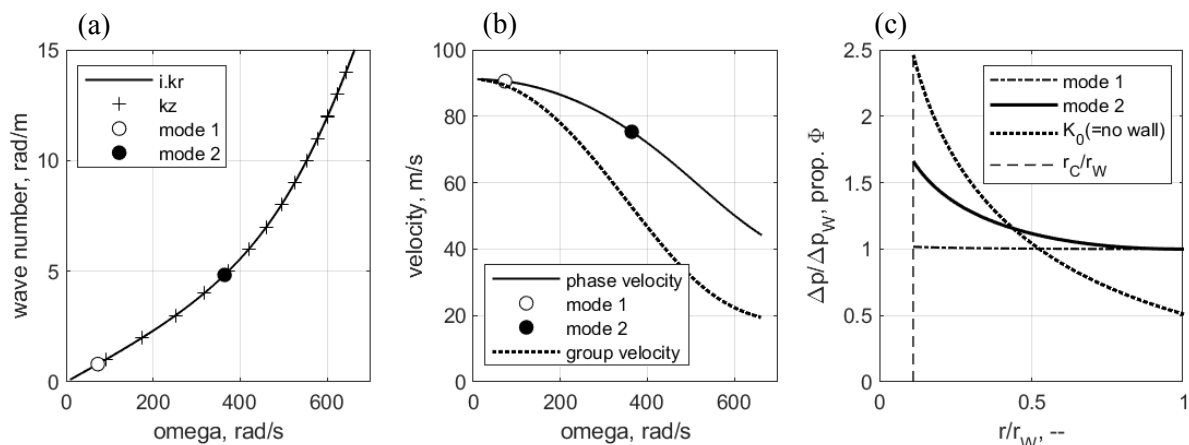
2.2. Quantitative example

The theory sketched in 2.1 may be illustrated using quantitative data comparable to the pulsation reported in [3] and presented as case 2a in Table 2. The basic assumptions are listed in Table 1. The example concentrates on the breathing pulsation ($n=0$) with wavelength $2L_c$. As demonstrated in [13], this is the way the pulsation shows in the simplified theory; the $n=2$ mode is not considered because it plays no role in the synchronous pulsation.

Table 1. Parameter input for quantitative example

Runner/ DT cone diameter	D_2 / D_W	0.30 / 0.36	m
Runner speed	n	24.3	1/s
Optimum / swirl-free/ test discharge	$Q_{opt} / Q_{no-rope} / Q$	0.523 / 0.539 / 0.418	m^3/s
Downstream angular momentum flux	T_2	109.6	kgm^2/s^2
Circulation	Γ	1.646	m^2/s
Cavity diameter / length	D_C / L_C	0.04 / 0.65	m
Axial / peripheral velocity	W / V_C	4.21 / 13.17	m/s

The dispersion relation for a uniform cavitating vortex with the properties given in Table 1 is shown in Figure 3(a). The diagram confirms the almost identical radial and axial wavenumbers due to $k \ll k_z$. Note that the acoustic wave celerity c (assumed 1400m/s) has almost no effect on the result. For the expected mode shape of the upper-part-load pulsation ('mode 2' in the Figure 3, 2 quarter waves within length L_C), corresponding to $k_z \approx \pi/L_C$, the dispersion relation yields a frequency of 57.9Hz, or 2.38 times runner frequency. The ordinary low-frequency mode 1, assuming a diffuser with average inertance, is also indicated for comparison.

**Figure 3.** Dispersion relation (a), phase and group velocities(b), velocity potential/pressure amplitude profile (c)

The evaluation reveals a couple of remarkable facts; firstly, the phase velocity is frequency-dependent due to the nonlinear dispersion relation. As shown in diagram (b), the quasi-steady 'wave velocity' holds for the ordinary part-load pulsation (mode 1), but not for the higher frequency of the high-partial load pulsation. Another observation is more important for understanding this pulsation: the radial distribution of the velocity potential (and, at the same time, the amplitude of pressure pulsation), shown in diagram (c), deviates considerably from the low-frequency case. The elevated wavenumbers of mode 2 are already sufficient to produce a significant radial gradient of pressure amplitude. The mode shape for the radially unbounded case, also indicated in diagram (c), would have even steeper gradient.

2.3. Interaction with vortex precession

Contrary to the assumptions in 2.1, in case of the partial-load vortex the vortex axis is not straight but permanently distorted into a helical shape. The distance between any single point at the draft tube wall (such as a pressure sensor) and the draft tube rope thus undergoes a periodic variation. As shown in Figure 3(c), the amplitude of the $n=0$ pressure pulsation mode strongly decreases with increasing distance from the vortex axis. In order to simulate the pressure variation in a point W at the wall of the draft tube cone, the narrow-band pressure fluctuation with frequency f_c therefore has to be multiplied by a harmonic weighting function whose period $t_v=1/f_v$ corresponds to the precession frequency f_v .

For simplicity, both periodic functions will in the following example be represented by their fundamental frequencies only; the formalism can easily be applied to harmonics of f_c and f_v .

Pressure pulsation at any point W in the same cross section:

$$\tilde{p} = \hat{p} \cdot \cos \omega_c t \quad (7)$$

Linearized influence of relative vortex location (distance from draft tube wall) on amplitude \hat{p} , with angle θ indicating the peripheral location of sensor W

$$\hat{p}(\theta) = p_0 + p_1 \cdot \cos(\omega_v t - \theta) \quad (8)$$

The pressure variation at any point W caused by the synchronous pulsation centred at the rope is obtained by inserting (8) in (7), and applying the multiplication theorem for the cosine function

$$\tilde{p} = p_0 \cdot \cos \omega_c t + (p_1 / 2) \cdot \cos[(\omega_c - \omega_v)t + \theta] - (p_1 / 2) \cdot \cos[(\omega_c + \omega_v)t - \theta] \quad (9)$$

This process generates a synchronous pulsation with frequency ω_c and two asynchronous pulsations. For locations in one plane, the phase of $\omega_c - \omega_v$ differs like the negative position angle ($-\theta$), while the phase of $\omega_c + \omega_v$ corresponds to the position angle θ , as in Arpe's [4] test results shown in Figure 6. The asynchronous sidebands in the wall pressure spectrum are thus a local effect resulting from the periodic displacement of the vortex, and negligible outside of the draft tube cone.

3. Experimental evidence

3.1. Typical occurrence

According to published data in Table 2, the oscillation occurs in turbines of high specific speed in a typical narrow load range of approximately $0.7 < Q/Q_{opt} < 0.85$. In the selected points the pulsation is a stationary oscillation (Figure 4) that induced some authors to call it a resonance; it seems to be a condition of slight instability (self-excited oscillation). In neighbouring load conditions, short bursts of the pulsation (Figure 5) indicate a slightly damped eigenmode excited by spontaneous flow variations.

Table 2. Test conditions with strong high-partial-load pulsation from literature

Case	Ref.	n_{Qopt}	ϕ/ϕ_{opt}	ψ/σ	f_c/n	f_c/f_v	Name
1	Jacob et al. [2], 1990	82	0.79	~ 0.18	1.28	4.6	80% load oscillation
2a	Dörfler [3], 1993	108	0.71	0.32	2.09	8.0	
2b	Dörfler [3], 1993	108	0.76	0.32	2.31	6.8	
3	Arpe [4], 2003	89	0.70	0.45	2.50	6.7	
4	Koutnik et al., [7], 2006	67.5	0.74	nn	~ 2.8	8.3	Higher Part Load P P
5	Nicolet et al., [8], 2010	79	0.83	~ 0.32	3.04	~ 7.5	UPL press. fluct.
6	Dörfler et al. [1], 2013	108	0.80	0.31	2.63	8.2	80% pulsation
7	Kuznetsov et al. [6], 2014	73.6	0.82	0.22	1.90	6.3	UPL unsteady phen.
8	Bouloc et al. [6], 2016	nn	0.78	nn	3.54	16.3	UPL resonance

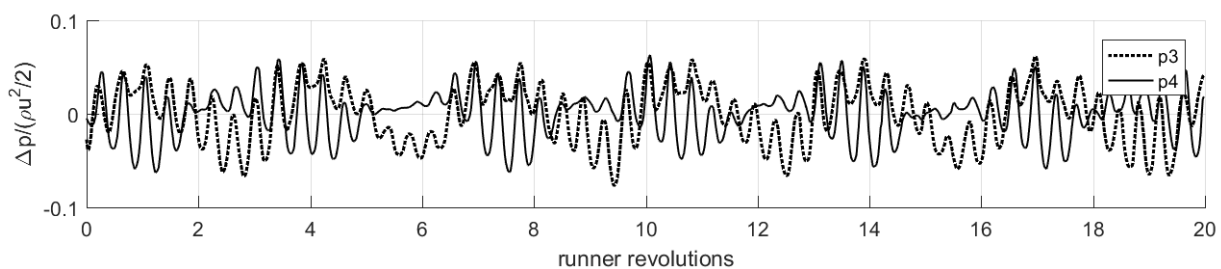


Figure 4. Example for stationary process at 2 opposite locations (Table 2/case 6, same test as Figure 1)

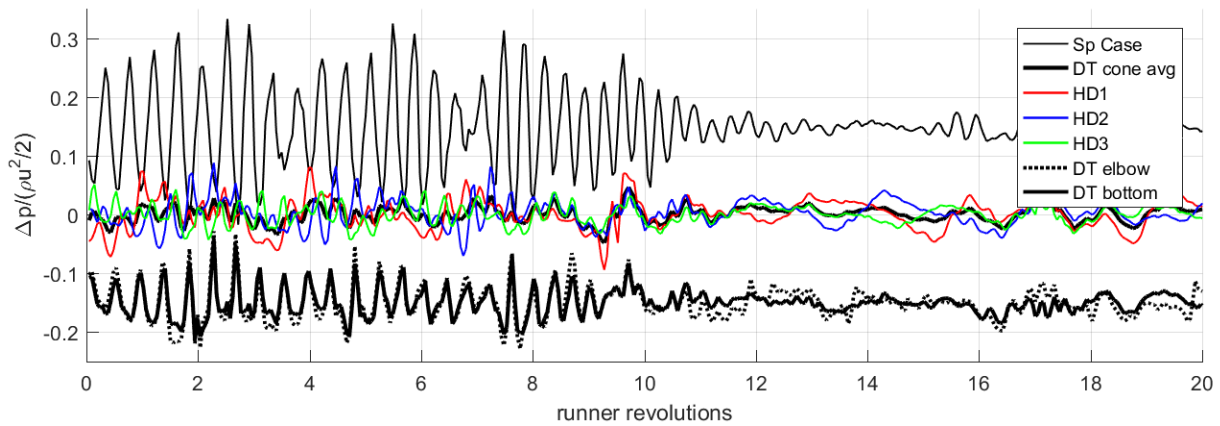


Figure 5. Example for damped oscillation (Table 2/case 2b, test series in ref. [3], data courtesy Andritz Hydro)

3.2. Frequency characteristics

For typical frequencies see Table 2. In all reported cases, the frequency f_c increases with increasing load Q/Q_{opt} , and with increasing cavitation number σ . Both effects result from a corresponding change of the phase velocity on the cavitating vortex.

3.3. Peripheral synchronism of main frequency band

The main frequency band with centre frequency f_c is the band which penetrates into the penstock and draft tube end. The pulsation at frequency f_c in all peripheral locations of one draft tube cone cross section close to the runner is synchronous. This feature has been mentioned by several researchers [2][4][6][7][12]; an example with data from [4] is shown in Figure 6. The synchronism is in accordance with equ. (9). It indicates that the high-partial load pulsation has the mode shape $n=0$ (breathing mode).

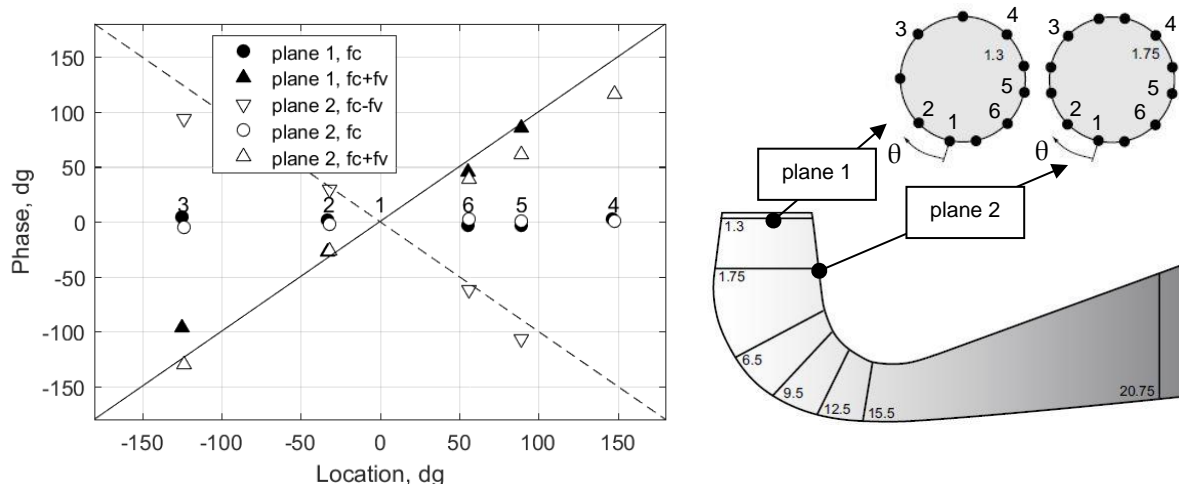


Figure 6. Phase of high-partial-load frequency bands against point 1, measurement locations (data Arpe [4], Mauri [5])

3.4. Peripheral phase characteristics of side bands

As demonstrated in Figure 6, the phase relationships for the sidebands with frequencies f_c+f_v and f_c-f_v are in accordance with equation (9). Note that there is synchronism for f_c *within* each single plane, but not *between* planes 1 and 2, see next subsection.

3.5. Longitudinal phase characteristics

Phase relationships between various locations along the flow path are available from a few sources. In reference [6],[8], the oscillations in the spiral case and in the upper draft tube cone are approximately synchronous. This is also the case in ref. [3], as shown in Figure 4.

In the detailed study of Arpe [4], the phase across the turbine is not disclosed but may be reconstructed based on the four values in the high-pressure pipe. The phase along the draft tube is given for 7 cross sections, see Figure 7. Arpe's observation (case 3 in Table 2) reveals that the pressure pulsation at the upstream and downstream end of the axial draft tube section has roughly opposite phase, see Figure 7. This feature was also found in the analysis of the model test reported in ref. [3] (case 2a in Table2, and Fig. 5 above).

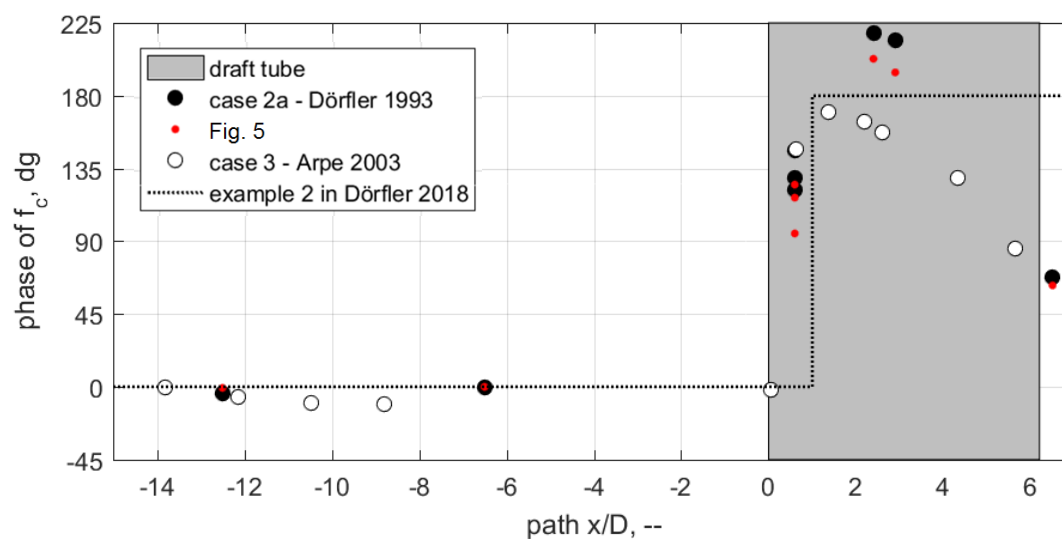


Figure 7. Phase of f_c against upstream pipe/draft tube entry, data from refs. [3], [4], [13]

Arpe [4] and some later researchers considered the pulsation in the draft tube cone to be a traveling wave and constructed, from the two planes shown in Figure 6, a longitudinal profile of phase velocity. There is some contradiction with the finding of a test rig eigenmode at the pulsation frequency, in the same study.

Indeed a more plausible interpretation would be a standing wave with a node and phase reversal of pressure between the two planes in the cone. This concept is elaborated in some detail in Part II of this study [13], and sketched in Figure 7. In this context, note the opposite phase between the upstream and downstream pressures in Figure 5, and the reduced amplitude at the draft tube cone in the same figure.

3.6. Longitudinal amplitude characteristics

In some tests [3][6][8], the amplitude measured at the wall of the draft tube cone was smaller than the one at the turbine intake. In ref. [3][4], it was smaller than in the elbow region.

In connection with the phase characteristic (3.5), it would be interesting to know if there is a pressure node somewhere along the cone (together with the phase change by $\sim 180^\circ$). Unfortunately this cannot be checked because it would have required a sufficient number of sensors distributed along some meridian in the cone region. Even Arpe's study [4], with a very large number (>100) of sensors on the draft tube surface, does not answer this question because the phase jump of 150° between the two measurement planes shown in Figure 6 is not resolved any further and no amplitudes are disclosed.

3.7. Visual/optical observation

Visual observation in case of sustained oscillations (for instance, ref. [3][7][8]) shows a cavity with clear surface and small diameter (sometimes less than 10% of draft tube diameter).

Elliptic deformation of the cavity cross section has been reported in several cases [7],[8]. The authors of the respective papers conjectured that this shape of deformation (i.e., the $n=2$ mode) plays a role in the oscillation mechanism. This assumption cannot be maintained because of two facts:

- (a) Peripheral synchronism of the pressure pulsation implies mode $n=0$. In case of a dominating $n=2$ mode, the phase would have to change by 4π around the circumference, see equation (1)
- (b) The measured cavity volume is found to pulsate [8], its phase being approximately opposed to the system pressure, as in Figure 8. An $n=2$ mode does not produce cavity volume changes.

Nicolet et al. [8] obtained the projected size AW of a short piece of the upper portion of the vortex by image processing, together with two wall pressure signals in the cone. 30 cycles of the signals are displayed in ref. [8]. Figure 8 shows AW ($\sim V$) and the average of the two pressures at $f_c=36\text{Hz}$, after high-pass-filtering. Negative work $W_{\text{cycle}}=\int p \cdot dV$ results for most of the cycles but this concerns only the small fraction of the cavity that was observed. With the amount of published data it is difficult to draw an unambiguous conclusion. In presence of rotating elliptical deformations, the void fraction cannot correctly be evaluated using single direction imaging; Pennings et al. [10] therefore used two simultaneous orthogonal views in order to separate the various peripheral modes. Also, the wall pressure is not a direct measure for the energy transport because of the radial gradient of pressure fluctuation (see Figure 3(c)) on a cavitating vortex, in case of high frequency.

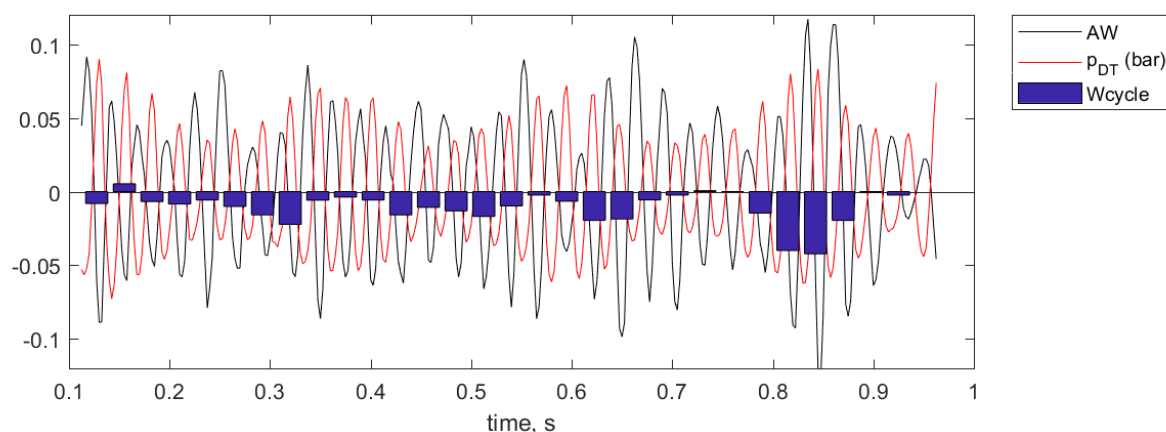


Figure 8. f_c component of draft tube wall pressure, partial vortex volume AW , and cycle work, based on ref. [8]

3.8. Additional observations (mechanical effects)

Kuznetsov et al. [6] measured the variation of axial thrust in the model test. The spectrum of axial thrust is approximately proportional to the spiral casing pressure. This case (no. 7 in Table 2) is also remarkable because the pulsation occurred, with similar features including axial vibration, at the large prototype turbine.

Significant pulsation of axial thrust was also observed in a model test campaign reported by Bouloc et al. (case 8 in Table 2 and [12]) whose main focus was the discrimination of azimuthal mode shapes of draft tube pressure. Their evaluation confirmed that the observed upper-part-load pulsation was limited to the $n=0$ mode. Accordingly it did not produce substantial variations of radial thrust. Evaluation of onboard measurement of unsteady runner blade stress in the critical location yielded only marginal contribution of the upper-part-load pulsation.

4. Excitation mechanism

Many observed properties of the upper-part load pulsation suggest that it is not a forced but a self-excited oscillation. Main indications are its abrupt onset in a narrow range of operation, and the particular dependency of its frequency on the draft tube pressure level. Like the full-load instability, it occurs in a load range where high absolute mass-flow gain can serve as a destabilizing agent. Also, its occurrence in turbines with high specific speed hints to the fact that low hydraulic resistance of the runner is essential for instability. These ideas are confirmed in Part II of this study [13].

5. Conclusions

Being synchronous over one cross section of the draft tube, the upper-part-load pulsation has to be understood as a breathing oscillation of the cavitating partial-load vortex. Oval deformations of the cavity, occasionally observed, do not show up in the phase of wall pressure; they are therefore not relevant in the oscillation mechanism.

The side bands in the spectra of draft tube pressure are a by-product of the vortex precession and the radial gradient of the pressure amplitude; this is confirmed by their asynchronous phase.

The available observations permit a simple interpretation of this pulsation based on the second-lowest eigenmode. Its preferred occurrence at the edge of part-load cavitation and in low-head turbines results from the fact that it needs conditions with sufficient mass-flow gain and very little damping.

The acoustic model, a novel approach in the context of the draft tube vortex, has some merits in providing the explanation of the frequency sidebands. Also, it gives a late and unexpected justification for the conventional practice to treat low-frequency pulsations in the draft tube like plane waves. On the other hand, no analytical method is available for its application in an environment with axially non-uniform pressure and cross section. For that reason, and because the side bands are not relevant in terms of the system-wide synchronous pulsation, the eigenvalue examination in Part II of this study [13] neglects the two-dimensional aspects of the acoustic model of section 2.

6. Acknowledgement

The author is indebted to Andritz Hydro for having provided model test results displayed in Figures 5 and 7.

Nomenclature

A	cross-section area [m ²]	α	coefficient in ϕ [-]
c	speed of sound [m/s]	Φ	amplitude of radial potential [m ² /s]
D, D ₂	diameter [m], ... at runner exit	ϕ	radial term of disturbance potential [-]
E	specific energy [J/kg]	φ	velocity potential [m ² /s]
f	frequency [Hz]	θ	peripheral coordinate [rad]
g	gravity acceleration [m/s ²]	ρ	fluid density [kg/m ³]
h	piezometric head [m]	σ	cavitation number [-] IEC 60193
i	imaginary unit [-]	ω	angular frequency [rad/s]
I _n , K _n	modified Bessel functions [-]	Ω	angular frequency at $r=r_c$ [rad/s]
k	Wave number [rad/m]	ψ	head coefficient
L	length [m]		
n	azimuthal wave number [-]	Indexes	
n	runner rotation frequency [Hz]	C	cavity surface, UPL frequency
p	static pressure [Pa]	DT	draft tube
Q	discharge [m ³ /s]	ED, QE	references as per IEC 60193
r	radius [m]	n	for azimuthal mode n
t	time [s]	opt	at best efficiency point
u	velocity variation [m/s]	r	radial direction

V	volume of cavity [m ³]	V	vortex precession
W	mean axial velocity [m/s]	W	draft tube wall
W	mechanical work [W], in Fig. 8	z	axial direction
x	path length (0 at draft tube intake)	θ	peripheral direction

References

- [1] Dörfler P K, Sick M and Coutu A 2013, *Flow-Induced Pulsation and Vibration in Hydroelectric Machinery*, London: Springer, sections 2.2.5 and 7.2.1
- [2] Jacob Th and Prenat J-E 1990, Generation of hydro-acoustic disturbances by a Francis turbine model and dynamic behavior analysis, *Proc. 15th Symp IAHR Section Hydr Machinery and Cavitation* (Belgrade)
- [3] Dörfler P K 1993, Observation of pressure pulsations at high partial load on a Francis model turbine with high specific speed, *IAHR Work Group 1 (The Behavior of Hydraulic Machinery under Steady Oscillatory Conditions) 6th Meeting*, Lausanne 1993, also in: *Hydropower & Dams*, January 1994
- [4] Arpe J A 2003, *Analysis of the wall pressure field in an elbow-type Francis draft tube* (in French), PhD thesis no. 2779, EPFL Lausanne (CH)
- [5] Mauri S 2002, *Numerical simulation and flow analysis of an elbow diffuser*, PhD thesis no. 2527, EPFL Lausanne (CH)
- [6] Kuznetsov I, Zakharov A, Arm V and Akulaev R 2014, Model and prototype investigations of upper partial load unsteady phenomena on the Francis turbine designed for head up to 120 m, *27th Symp IAHR Section Hydr Machinery and Cavitation* (Montreal, 2014)
- [7] Koutnik J, Krüger K, Pochyly F, Rudolf P and Haban V 2006, On cavitating vortex rope form stability during Francis part load operation, *IAHR WG Cavitation and Dynamic Problems in Hydraulic Machinery and Systems* (Barcelona, 28-30 June 2006)
- [8] Nicolet C, Zobeiri A, Maruzewski P and Avellan F 2010, On the upper part load vortex rope in Francis turbine: Experimental investigation, *IAHR 25th Symp. Hydr Machinery and Systems* (Timisoara, 2010)
- [9] Bosschers J 2008, Analysis of inertial waves on inviscid cavitating vortices in relation to low-frequency radiated noise, *Proc. WIMRC Cavitation Forum*, Warwick University (UK)
- [10] Pennings P C, Bosschers J, Westerweel J and van Terwisga T J C 2015, Dynamics of isolated vortex cavitation, *J. Fluid Mech.*, vol. 778, pp. 288_313. Cambridge University Press 2015
- [11] Dörfler P K 1982, *System oscillations excited by the Francis turbine's part load vortex core: mathematical modeling and experimental verification*, PhD thesis (in German) TU Wien (AT), English translation (2013) on researchgate.net
- [12] Bouloc F, Guillozet J, Duparchy F, Lowys P-Y and Duparchy A, 2016, Mechanical risks prediction on Francis runner by Spatial Harmonic Decomposition, *IAHR 28th Symp. Hydr Machinery and Systems* (Grenoble)
- [13] Dörfler P K 2018, Analysis of the Francis turbine upper-part-load pulsation, Part II – Mechanism of Self-Excitation, *IAHR 29th Symp. Hydr Machinery and Systems* (Kyoto)